

UC Berkeley

UC Berkeley Previously Published Works

Title

Anomalous Shape Evolution of Ag<sub>2</sub>O<sub>2</sub> Nanocrystals Modulated by Surface Adsorbates during Electron Beam Etching

Permalink

<https://escholarship.org/uc/item/87c0b73m>

Journal

Nano Letters, 19(1)

ISSN

1530-6984

Authors

Zhang, Qiubo

Gao, Guoping

Shen, Yuting

et al.

Publication Date

2019-01-09

DOI

10.1021/acs.nanolett.8b04719

Peer reviewed

1 Anomalous shape evolution of Ag<sub>2</sub>O<sub>2</sub>  
2 nanocrystals modulated by surface  
3 adsorbates during electron beam etching

4 Qiubo Zhang<sup>†‡</sup>, Guoping Gao<sup>‡</sup>, Yuting Shen<sup>†±</sup>, Xinxing Peng<sup>‡</sup>, Junyi  
5 Shangguan<sup>‡</sup>, Yu Wang<sup>‡</sup>, Hui Dong<sup>†</sup>, Karen Bustillo<sup>§</sup>, Linwang Wang<sup>‡</sup>, Litao Sun<sup>†\*</sup>  
6 and Haimei Zheng<sup>¶||</sup> \*

7

8 <sup>†</sup> SEU-FEI Nano-Pico Center, Key Laboratory of MEMS of Ministry of Education,  
9 Collaborative Innovation Center for Micro/Nano Fabrication, Device and  
10 System, Southeast University, Nanjing 210018, P. R. China.

11 <sup>‡</sup> Materials Science Division, Lawrence Berkeley National Laboratory,  
12 Berkeley, California 94720, United States

13 <sup>±</sup> College of Physics and Electronic Engineering, Changshu Institute of  
14 Technology, Changshu 215500, P. R. China.

15 <sup>§</sup> National Center for Electron Microscopy, Molecular Foundry, Lawrence  
16 Berkeley National Laboratory, Berkeley, California, 94720, United States

17 <sup>||</sup> Department of Materials Science and Engineering, University of California,  
18 Berkeley, Berkeley, California, 94720, United States

19 ABSTRACT: An understanding of nanocrystal shape evolution is significant for  
20 the design, synthesis and applications of nanocrystals with surface-enhanced  
21 properties such as catalysis or plasmonic. Surface adsorbates that selectively  
22 adhere to certain facets may strongly affect the atomic pathways of  
23 nanocrystal shape development. However, it is a great challenge to directly

24 observe such dynamic processes in situ with high spatial resolution. Here, we  
25 report the anomalous shape evolution of  $\text{Ag}_2\text{O}_2$  nanocrystals modulated by  
26 the surface adsorbates of Ag clusters during electron beam etching, which is  
27 revealed through in situ transmission electron microscopy (TEM). In contrast  
28 to the  $\text{Ag}_2\text{O}_2$  nanocrystals without adsorbates, which display the near-  
29 equilibrium shape throughout the etching process,  $\text{Ag}_2\text{O}_2$  nanocrystals with  
30 Ag surface adsorbates show distinct facet development during etching by  
31 electron beam irradiation. Three stages of shape changes are observed: a  
32 sphere-to-a cube transformation, side etching of a cuboid, and bottom  
33 etching underneath the surface adsorbates. We find that the Ag adsorbates  
34 modify the  $\text{Ag}_2\text{O}_2$  nanocrystal surface configuration by selectively capping  
35 the junction between two neighboring facets. They prevent the edge atoms  
36 from being etched away and block the diffusion path of surface atoms. Our  
37 findings provide critical insights into the modulatory function of surface  
38 adsorbates on shape control of nanocrystals.

39 KEYWORDS: *In situ* TEM, shape evolution, surface adsorbates,  $\text{Ag}_2\text{O}_2$   
40 nanocrystal, electron beam etching.

41

42 Shape control of nanocrystals has been a significant topic since it directly  
43 impacts the physical and chemical properties of nanocrystals in catalysis,<sup>1, 2</sup>  
44 photonics,<sup>3, 4</sup> energy conversion<sup>5-7</sup> and other applications.<sup>8-11</sup> For a  
45 nanocrystal, the equilibrium shape evolution can be predicted by the Wulff  
46 construction theory where the rate of each individual facet change is

47 dependent on the different surface facet energy.<sup>12-14</sup> However, the  
48 nanocrystal surface energy can be modified by introducing surfactants,  
49 polymeric molecules or other adsorbates on the nanocrystal surface.<sup>15</sup> These  
50 surface agents affect the relative rate changes of different facets through  
51 selective capping or providing preferential atomic paths of shape evolution.<sup>15</sup>

52

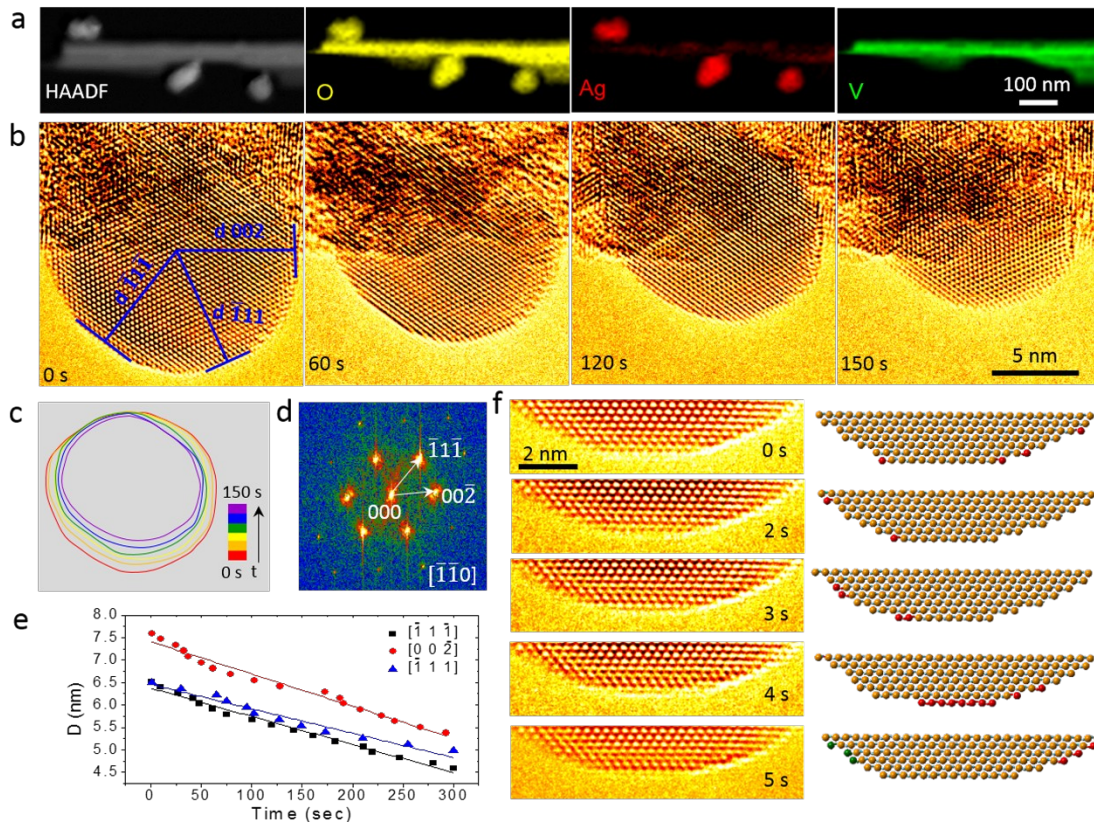
53 Small adsorbates with strong stability can alter the energy and reactivity of a  
54 crystal surface by forming a 'capping' layer,<sup>16</sup> which has been considered as  
55 a new class of effective shape controller for nanocrystals.<sup>15</sup> For instance, it  
56 was revealed that Ag<sup>+</sup> ions can promote the formation of {111} facets of Pt  
57 nanocrystals.<sup>15,17</sup> Halides prefer to adsorb on the {100} facets of Pd and Rh  
58 to facilitate the formation of Pd and Rh nanocubes.<sup>18, 19</sup> Understanding the  
59 microscopic mechanisms of surface adsorbates in shape control of  
60 nanocrystals is significant to the functional design and shape control of  
61 nanocrystals. In this regard, much work has been dedicated to the *in situ*  
62 study of the nanocrystal shape evolution.<sup>20, 21</sup> For example, we previously  
63 investigated the facet development of Pt nanocrystals under the influence of  
64 surface ligands during growth.<sup>20, 21</sup> Ye et al. studied the non-equilibrium  
65 shape evolution of individual gold nanocrystals during oxidative etching.<sup>21</sup>  
66 However, how surface adsorbates influence the atomic pathways of non-  
67 equilibrium shape evolution during etching processes is still far from well  
68 understood.

69 Electron beam irradiation has been used to etch materials with nanometric<sup>22-</sup>  
70 <sup>25</sup> or subnanometric<sup>26-28</sup> precision. The etching process can be monitored in  
71 the TEM in real time, which allows one to study the impact of surface  
72 adsorbates on shape evolution of nanocrystals directly.

73 Here, we use *in situ* TEM to study the influences of Ag surface adsorbates on  
74 shape evolution of Ag<sub>2</sub>O<sub>2</sub> nanocrystals during electron beam etching. Since  
75 Ag surface adsorbates are much more stable than the Ag<sub>2</sub>O<sub>2</sub> nanocrystal  
76 under electron beam irradiation,<sup>29</sup> the atoms capped by surface adsorbates  
77 may be protected from being etched away. The Ag<sub>2</sub>O<sub>2</sub>/Ag samples were  
78 prepared *in situ*. First, AgVO<sub>3</sub> nanorods were synthesized by a hydrothermal  
79 method.<sup>30</sup> Then, Ag<sub>2</sub>O<sub>2</sub> nanocrystals were formed on the surface of AgVO<sub>3</sub>  
80 nanorods using a low flux electron beam and an oxidation treatment  
81 (Supplementary Text; Figure 1a and Figure S1-3). Cs-corrected TEM (FEI  
82 Titan 80-300) operating with an acceleration voltage of 300 kV and with a  
83 parallel electron beam (current density  $\sim 2.3 \times 10^6$  A·m<sup>-2</sup>) was used for the  
84 study. The etching of Ag<sub>2</sub>O<sub>2</sub> nanocrystals was initiated by electron beam  
85 irradiation. The entire etching process was captured with atomic resolution  
86 and in real time. The results show that the Ag surface adsorbates have a  
87 modulatory function, which includes both selective capping on the surface of  
88 Ag<sub>2</sub>O<sub>2</sub> nanocrystals and blocking of the diffusion path of adatoms. The effects  
89 of surface adsorbates should be considered for the fabrication of  
90 nanomaterials with different non-equilibrium shapes.

91

## 92 Result and Discussion.



93

94 **Figure 1.** Near-equilibrium shape evolution of a  $\text{Ag}_2\text{O}_2$  nanocrystal during  
 95 electron beam etching. (a) HAADF-STEM image and EELS maps of individual  
 96  $\text{AgVO}_3$  nanorod decorated with  $\text{Ag}_2\text{O}_2$  particles. (b) Sequential HRTEM images  
 97 (false color) show the real-time shape evolution of a  $\text{Ag}_2\text{O}_2$  nanocrystal  
 98 during electron beam etching. Images are extracted from movie S1. (c) The  
 99 corresponding time-labeled contours indicate that the sphere-like shape  
 100 persists during the etching process. (d) The FFT pattern of the  $\text{Ag}_2\text{O}_2$   
 101 nanocrystal in (b). (e) The measured average distance from the center of  
 102 nanocrystal to each facet as a function of time. (f) *In situ* electron beam  
 103 etching details of the outermost  $(111)$  facet of  $\text{Ag}_2\text{O}_2$ . HRTEM images are

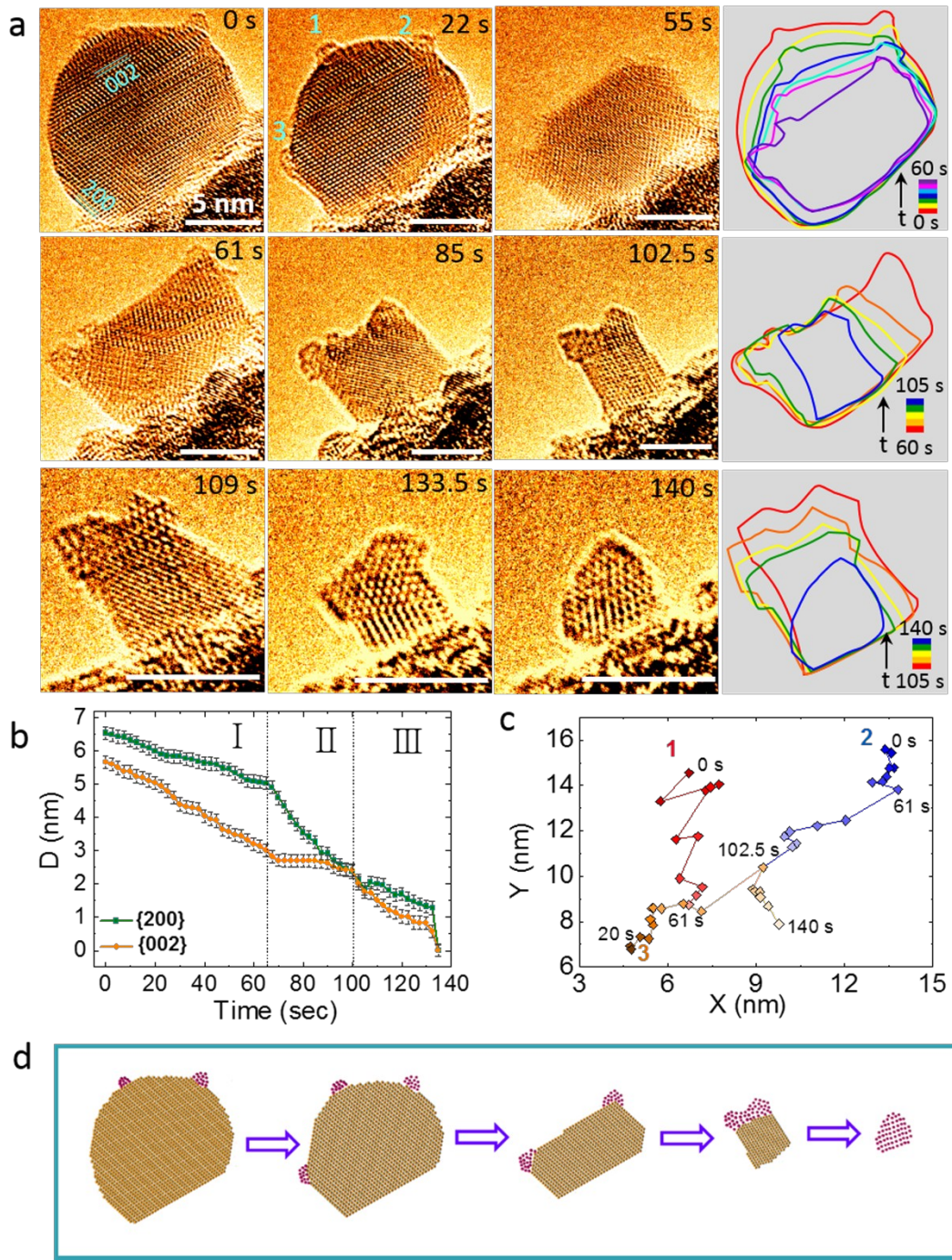
104 listed on the left and the corresponding stick-and-ball models are displayed  
105 on the right. The red balls indicate the atoms to be removed in the next  
106 frame, and the green balls indicate the newly appearing adatoms in this  
107 frame.

108

109 Figure 1 shows that the typical etching of  $\text{Ag}_2\text{O}_2$  nanocrystals without surface  
110 adsorbates follows the near-equilibrium shape evolution. The electron energy  
111 loss spectra (EELS) maps of  $\text{Ag}_2\text{O}_2$  nanocrystals supported on  $\text{AgVO}_3$   
112 nanorods show that these nanoparticles contain Ag and O elements; the V  
113 element only exists in  $\text{AgVO}_3$  nanorods (Figure 1a, Figure S3; see more  
114 details in Supplementary Text). High resolution transmission electron  
115 microscope (HRTEM) images (Figure 1b) and the corresponding fast Fourier  
116 transform (FFT) pattern show that the crystal structure of  $\text{Ag}_2\text{O}_2$  nanocrystal  
117 is monoclinic (Table S1; also see Figure S4 for more detailed structural  
118 characterization). Figure 1b shows the real time shape evolution of a  $\text{Ag}_2\text{O}_2$   
119 nanocrystal along the  $[\bar{1}\bar{1}0]$  viewing axis during etching. There is no obvious  
120 change in the crystal structure while the particle size reduces gradually, and  
121 the sphere-like shape is maintained throughout the entire etching process.  
122 The original HRTEM images of Figure 1b are shown in Figure S5. To better  
123 understand the details of etching, we construct time-labeled contour plots  
124 with equal time intervals (Figure 1c). The results show that etching of the  
125 nanocrystal occurs mostly in the upper part with the exposed surface. We  
126 quantified the evolution of the nanoparticle shape by tracking the

127 propagation of different facets. We first determine the crystal center of the  
128  $\text{Ag}_2\text{O}_2$  particle (Figure S6) and measure the distance from the center of the  
129 crystal to these three facets: (002),  $\{110\}$ ,  $\{111\}$  (Figure 1b). The distances as a  
130 function of time are plotted in Figure 1e. The etching rate of each facet  
131 (slope of each plot) is roughly proportional to their surface free energy  
132 ((002)~1.98 eV per Ag atom,  $\{110\}$ ~1.57 eV per Ag atom and  $\{111\}$  ~1.86 eV per Ag  
133 atom) as shown in Table. 1. This suggests that the etching process is near-  
134 equilibrium, as predicted by Wulff construction theory. The atomic pathways  
135 of etching on  $\{110\}$  facet are shown in Figure 1f. First, some atoms at the atomic  
136 steps with fewer neighbors are removed preferentially (0-3 s). Subsequently,  
137 atoms in the outmost layer of  $\{110\}$  facet are completely removed (4 s). Due to  
138 surface diffusion some atoms (marked by green balls) can be adsorbed at  
139 the steps to “heal” the defects. The subsequent etching of  $\{111\}$  facet (Figure  
140 S7) and the etching of  $\{110\}$  facet (Figure S8) show similar trends. Therefore,  
141 the shape evolution of  $\text{Ag}_2\text{O}_2$  nanocrystal without surface adsorbates is near-  
142 equilibrium - dominated by surface free energy and modified by surface  
143 diffusion of adatoms.





144

145 **Figure 2.** Anomalous shape evolution of a  $\text{Ag}_2\text{O}_2$  nanocrystal with Ag surface  
 146 adsorbates. (a) Sequential HRTEM images (false color) show the real-time  
 147 shape evolution of the  $\text{Ag}_2\text{O}_2$  nanocrystal with Ag surface adsorbates during  
 148 etching under electron beam. Images are extracted from video S2. The

149 etching process can be divided into three regimes: spherical-to-cuboidal  
150 shape transformation, side etching and bottom etching. The corresponding  
151 time-labeled contours in each regime are listed in the right column. The  
152 original HRTEM images are shown in Figure S12. (b) The measured average  
153 distances from the center of nanocrystal to (200) and (002) facets as a  
154 function of time. Error bars indicate the standard deviation. (c) Migration  
155 trajectories of three surface adsorbates including a newly formed one. (d)  
156 Schematic illumination of the anomalous etching process.

157

158 Etching of  $\text{Ag}_2\text{O}_2$  nanocrystal with Ag surface adsorbates is very different  
159 from that of the regular  $\text{Ag}_2\text{O}_2$  nanocrystal with a clean surface. For example,  
160 a  $\text{Ag}_2\text{O}_2$  nanocrystal with the same monoclinic structure has two adsorbates  
161 on the surface of nanocrystal (Figure S9). Due to the small sizes and the  
162 dynamic nature of the clusters, we cannot directly determine the crystal  
163 structure of the surface adsorbates during etching. However, through HRTEM  
164 and EELS spectra of the remaining cluster, it is clear that the surface  
165 adsorbates are Ag clusters with hexagonal closest packed structure (Figure  
166 S11). Figure 2a shows the real-time shape evolution of a  $\text{Ag}_2\text{O}_2$  nanoparticle  
167 with Ag surface adsorbates during etching, and the corresponding time-  
168 labeled contours are listed in the right column.

169

170 Based on the characteristics of the shape changes, the etching process of a  
171  $\text{Ag}_2\text{O}_2$  nanocrystal with the Ag surface adsorbates can be divided into three

172 regimes: spherical-to-cuboidal shape transformation (0 s to 60 s), side  
173 etching (60 s to 105 s) and bottom etching (105 s to 140 s). At the initial  
174 stage, atoms at the steps with fewer neighbors are sputtered away  
175 preferentially, and some atoms diffuse on the surface randomly to heal  
176 defects (see Figure S13), which is similar to the etching of the nanoparticle  
177 with clean surface. Subsequently, the etching of (002) facet becomes faster  
178 and the sphere-like nanoparticle transforms to cuboid-like shape (22 s to 60  
179 s) as shown in Figure 2a. During this process, a new Ag cluster marked by  
180 number 3 formed probably due to the reduction of the  $\text{Ag}_2\text{O}_2$  through the  
181 formula:  $\text{Ag}_2\text{O}_2 \rightarrow \text{Ag} + \text{O}_2$ . Cluster 2 and cluster 3 remain stationary, while  
182 cluster 1 moves randomly and it eventually merges with the cluster 3 as  
183 indicated by the contours and migration trajectories in Figure 2c. In the  
184 second regime, the  $\text{Ag}_2\text{O}_2$  cuboid nanocrystal is pinned by the Ag clusters at  
185 the corners. Etching proceeds by gradually removing the side surface and  
186 there is almost no change in the vertical direction (Figure 2b). The method of  
187 determining the center of the particle (reference point) in Figure 2a is shown  
188 in Figure S14.

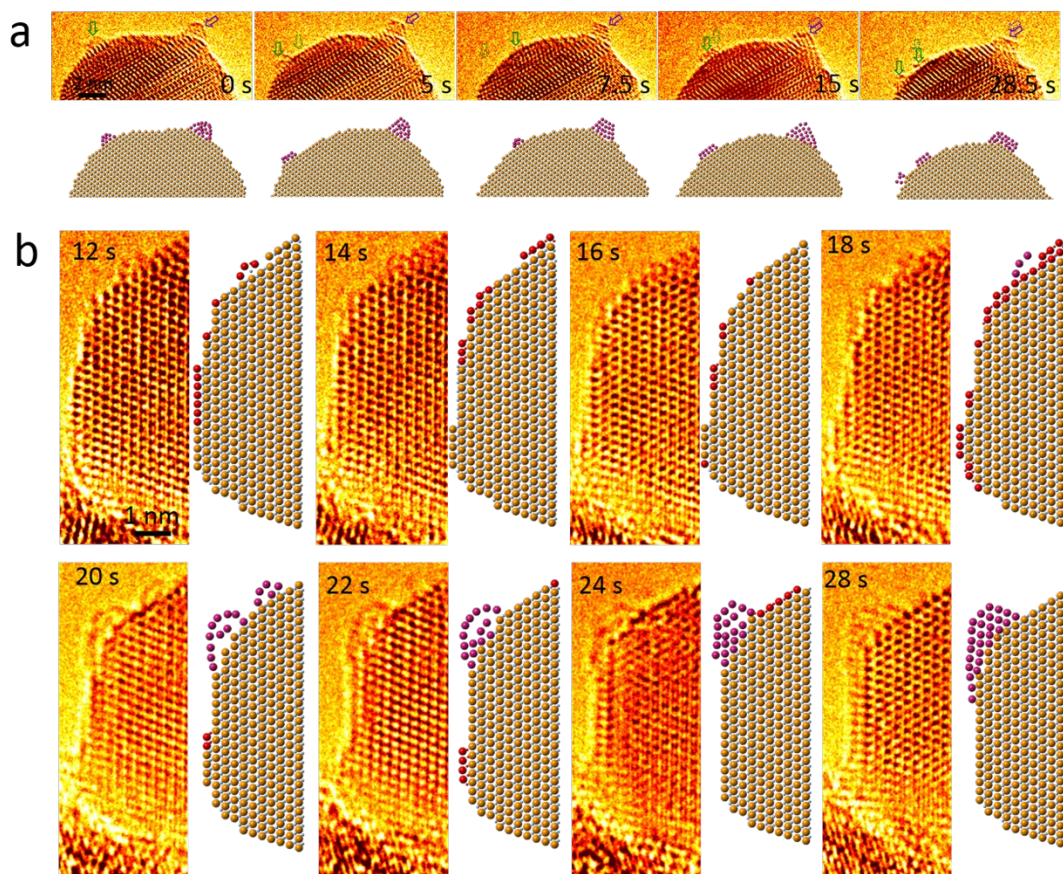
189  
190 The etching is mainly along the right side of the nanocrystal from 61s to 85  
191 s, but both sides are etched after 85 second; this observation will be  
192 discussed in more detail later in this report. In the end, the three Ag clusters  
193 are combined to form a large one. In the last regime, the top of the  $\text{Ag}_2\text{O}_2$   
194 nanocrystal is completely capped with a Ag cluster. Intuitively, with the  
195 protection of Ag cluster, the  $\text{Ag}_2\text{O}_2$  nanocrystal can only be etched from the

196 side. However, as the width decreases, the height also decreases accordingly  
197 likely due to minimization of the surface free energy of a certain volume,  
198 which is different from the case of the second sub-process (Figure 2b).  
199 Eventually, the  $\text{Ag}_2\text{O}_2$  nanocrystal is completely etched away, leaving only  
200 the surface adsorbates.

201 We further find that the etching rate of (200) and (002) facets is not  
202 proportional to their theoretical surface free energy ((200): 2.05 eV per Ag  
203 atom, (002): 1.98 eV per Ag atom; (220): 2.23 eV per Ag atom as listed in  
204 Table 1). Therefore, etching of the  $\text{Ag}_2\text{O}_2$  nanocrystal with Ag surface  
205 adsorbates is characterized by non-equilibrium shape transformation. The  
206 shape evolution process is highlighted in Figure 2d.

207





208

209 **Figure 3.** Selective capping and dynamics of Ag surface adsorbates on the

210  $\text{Ag}_2\text{O}_2$  nanocrystal. (a) Sequential HRTEM images (false color) and atomic

211 models show the movement of Ag surface clusters on the  $\text{Ag}_2\text{O}_2$  surface

212 during electron beam etching. The Ag clusters adsorbed at the junction

213 between the (200) and (002) facets terminals (marked by purple arrows) are

214 more stable than those on the (002) facets (marked by green arrows). (b)

215 Sequential snapshots of HRTEM images and atomic models show the *in situ*

216 growth of an Ag surface adsorbate and its adjustment function during

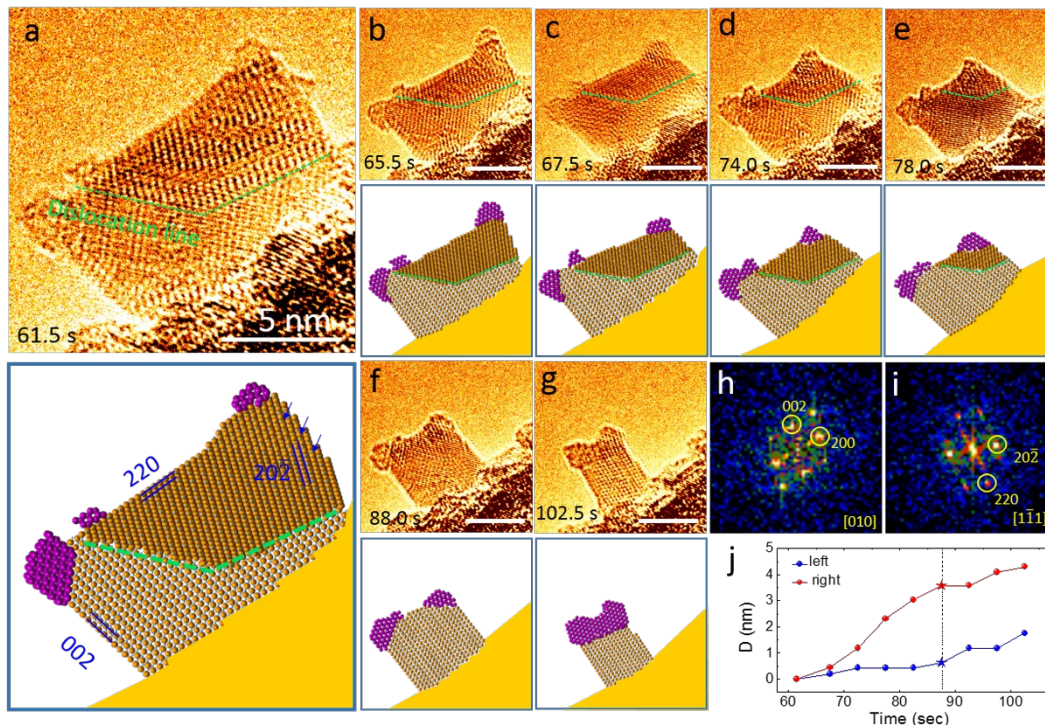
217 electron beam etching. The corresponding original HRTEM images are shown

218 in Figure S15.

219

220 To further study the microscopic mechanisms behind the anomalous shape  
221 evolution of  $\text{Ag}_2\text{O}_2$  nanocrystal, we focus on the influences of Ag surface  
222 clusters on the sphere-to-cuboid transformation. Figure 3a shows the Ag  
223 surface adsorbates on the  $\text{Ag}_2\text{O}_2$  nanocrystal surface while the nanocrystal is  
224 etched away. At the initial state, cluster 1 (marked by green arrow) sits on  
225 the (002) facet and cluster 2 (marked by purple arrow) is adsorbed at the  
226 junction between the (200) and (002) facets. Then, cluster 1 moves  
227 randomly on the (200) facet while the nanocrystal is etched away. It splits  
228 into two at 28 s and the right one quickly combines with cluster 2.  
229 Meanwhile, cluster 2 is almost stationary at the facet junction. The behavior  
230 of Ag clusters on the  $\text{Ag}_2\text{O}_2$  nanocrystal surface is likely due to the energy  
231 variations of different positions. For instance, the Ag cluster is fixed at the  
232 corner due to a high adsorption energy, while it moves randomly on the flat  
233 (002) surface without preferable location and eventually bonds with the  
234 atoms at the corners of the  $\text{Ag}_2\text{O}_2$  crystal. Figure 3b shows the formation of a  
235 new Ag cluster and how it affects the etching of different facets at the atomic  
236 level. From 12 s to 16 s, etching starts from the atomic steps and some atoms  
237 diffuse on the surface to form adsorbed atoms. These atoms come together  
238 to form a cluster (see details in frames between 18 s and 28 s). Before the  
239 cluster formation, two layers of (200) facet and three layers of (002) facet  
240 are etched (12-22 s). However, after the cluster formation, only the (002)  
241 facet is etched. Etching along the (200) facet is stopped, which is probably  
242 due to a Ag cluster that caps the atomic steps of (200) facet. The (002) facet

243 has two terminals, and even though the left terminal is capped with the Ag  
 244 cluster, etching can still proceed along the atomic steps at the right terminal.  
 245 Further etching leads to the conversion of a spherical nanocrystal to a  
 246 cuboid.  
 247



248  
 249 **Figure 4.** Asymmetric side etching of the cuboidal  $\text{Ag}_2\text{O}_2$  nanocrystal with Ag  
 250 surface adsorbates. (a-g) Sequential HRTEM images (false color) and the  
 251 atomic models show that the etching speed of the  $\text{Ag}_2\text{O}_2$  nanocrystal is faster  
 252 on the right side than the left. The atoms of Ag clusters are marked with  
 253 purple and the Ag atoms in  $\text{Ag}_2\text{O}_2$  nanocrystal are marked with orange. The  
 254 corresponding original HRTEM images are shown in Figure S16. (h) and (i)  
 255 are the corresponding FFT patterns of bottom part and top part, which are

256 separated by the dislocation line. (j) The measured distances from the center  
 257 of the nanocrystal to the left and right facets as a function of time.

258

259 Table 1. The calculated surface energy per Ag atom of different crystal  
 260 facets.

Facets	{00 2}	{ 113 }	{20 0}	{ 111 }	{ 111 }	{ 113 }	{ 220 }	{22 0}
Surface energy (eV)	1.98	2.01	2.05	1.57	1.86	2.32	2.40	2.23

261

262 As mentioned above, in the second regime of etching, the etching rate on  
 263 the right side of cuboidal  $\text{Ag}_2\text{O}_2$  nanocrystal is much faster than that on the  
 264 left side (61.5-88 s). After 88 s, the etch rates on both sides become similar.  
 265 Figure 4a shows the  $\text{Ag}_2\text{O}_2$  nanocrystal is divided into two parts by one  
 266 dislocation line. The corresponding FFT patterns (Figure 4h, i) of these two  
 267 parts indicate that they have the same crystal structure but along different  
 268 zone axes with the bottom along [010] and the top along [111]. As shown in  
 269 the atomic model in Figure 4a, the (200) facet on the left, (220) facet on the  
 270 top, and the (111) facet on the right side are highlighted.

271

272 We calculate the facet energy of a  $\text{Ag}_2\text{O}_2$  nanocrystal using density functional  
 273 theory (DFT) and the results are shown in Table 1. Comparing the surface  
 274 energy of the (200) facet (2.05 eV per Ag atom) and the (220) facet (2.23 eV  
 275 per Ag atom), the etching is preferential along the sides of  $\text{Ag}_2\text{O}_2$  nanocrystal



276 in order to reduce the surface energy. As shown in Figure 4a-e, there are no  
277 atomic steps on the left side while there are some on the right side as  
278 pointed by blue arrows. The atoms at the atomic steps have fewer neighbors,  
279 which may be etched away quickly. As the etching progresses, the  
280 dislocation line gradually moves to the corner until it disappears at 88 s  
281 (Figure 4a-e). At that moment, both sides of the crystal are {200} facets and  
282 the majority of atomic steps disappear (Figure 4f-g), resulting in almost the  
283 same etching rates on both sides. Figure 4j shows the distances from the  
284 crystal center to the left and right facet surfaces as a function of time. We  
285 first build a Cartesian coordinate system for the sequential images (Figure  
286 S17). The coordinate origin of Cartesian coordinate system is a characteristic  
287 position on the substrate, the x axis is parallel to the substrate, the positions  
288 on left and right sides are marked by yellow and blue lines, respectively.  $L_x$   
289 and  $R_x$  ( $x=0, 1, 2, 3, 4, 5, 6, 7, 8$ ) represent the distance from coordinate  
290 origin to the left and right sides, so we can use this feature position as a  
291 reference to study the motion on both sides of the nanocrystal.

292

293 **Conclusion.** In summary, we have observed the anomalous shape evolution  
294 of  $\text{Ag}_2\text{O}_2$  nanocrystals modulated by the surface adsorbates during the  
295 etching process under electron beam. The Ag surface adsorbates strongly  
296 influence the atomic pathways of  $\text{Ag}_2\text{O}_2$  nanocrystal etching. This work  
297 suggests potential strategies for controlling non-equilibrium shape  
298 transformation of nanocrystals with surface adsorbates. The ability to

299 directly observe the dynamic processes of nanocrystals at the atomic scale  
300 may assist the study and design of many other nanocrystals with novel and  
301 controlled shapes.

302

303 ASSOCIATED CONTENT

304 **Supporting Information.**

305 The supplementary text includes descriptions of the synthesis of  $\text{AgVO}_3$   
306 nanorods, preparation of  $\text{Ag}_2\text{O}_2$  nanocrystals, materials characterization, TEM  
307 observation, and density functional theory calculations. Figures include  
308 structural characterization and elemental composition of the as prepared  
309  $\text{AgVO}_3$  and  $\text{Ag}_2\text{O}_2$  samples, the schematic of growth route of  $\text{Ag}_2\text{O}_2$  particles  
310 on  $\text{AgVO}_3$  substrates, the raw HRTEM images corresponding to Figure 1(b),  
311 Figure 2(a), Figure 3 and Figure 4, the determination of crystal center, the  
312 detailed etching process of  $(\bar{1}\bar{1}\bar{1})$  and  $(\bar{1}11)$  facets of a  $\text{Ag}_2\text{O}_2$  nanocrystal  
313 with clean surface, the shape and structure evolution of Ag cluster during the  
314 etching process, the characterization of the remaining Ag cluster after  
315 electron beam etching, sequential images showing the movements of both  
316 sides of the nanocrystal, the calculation model and surface energy of each  
317 facets. Table S1 shows the crystal structure data for  $\text{AgVO}_3$ ,  $\text{Ag}_2\text{O}$ ,  $\text{Ag}_2\text{O}_2$ ,  
318  $\text{Ag}_2\text{O}_3$ ,  $\text{Ag}_3\text{O}_4$  and Ag. (PDF)

319

320 Near-equilibrium shape evolution process of a  $\text{Ag}_2\text{O}_2$  nanocrystal during  
321 electron beam etching. (AVI)  
322

323 Anomalous shape evolution process of a  $\text{Ag}_2\text{O}_2$  nanocrystal with Ag surface  
324 adsorbates. (AVI)  
325

326 AUTHOR INFORMATION

327 **Corresponding Author**

328 \* E-mail: [hmzheng@lbl.gov](mailto:hmzheng@lbl.gov); \*E-mail: [slt@seu.edu.cn](mailto:slt@seu.edu.cn);

329 **Author Contributions**

330 The manuscript was written through contributions of all authors. Q. Z., H. Z.  
331 and L. S. conceived the project. Q. Z. performed the *in situ* TEM imaging. G.  
332 G. performed the calculations. Q. Z., Y. S., X. P., Y. W., H. D., and L. W., carried  
333 out the data analysis. Q. Z., H. Z. and L. S. co-wrote the paper with all  
334 authors contributing to the discussion and preparation of the manuscript.

335

336 ACKNOWLEDGMENT

337 This work was funded by the U.S. Department of Energy (DOE), Office of  
338 Science, Office of Basic Energy Sciences (BES), Materials Sciences and  
339 Engineering Division under Contract No. DE-AC02-05-CH11231 within the in-  
340 situ TEM program (KC22ZH). The work at Southeast University was supported  
341 by the National Natural Science Foundation of China (Nos 51420105003,

342 11327901, 11525415, 11674052). Work at the Molecular Foundry was  
343 supported by the Office of Science, Office of Basic Energy Sciences, of the  
344 U.S. Department of Energy under Contract No. DE-AC02-05CH11231. Q. Z.  
345 acknowledges funding support from the China Scholarship Council  
346 (201606090071) and Scientific Research Foundation of Graduate School of  
347 Southeast University (YBPY1708). We thank Chengyu Song for his help with  
348 the Tecnai microscope set up.

349

## 350 ABBREVIATIONS

351 HRTEM, high resolution transmission electron microscope; EELS, energy-loss  
352 spectroscopy; FFT, fast Fourier transformation; DFT, density functional  
353 theory.

## 354 355 REFERENCES

- 356 1. Bell, A. T. *Science* **2003**, 299, 1688-1691.
- 357 2. Yan, W.; Mahurin, S. M.; Pan, Z.; Overbury, S. H.; Dai, S. *Journal of the American*  
358 *Chemical Society* **2005**, 127, 10480-10481.
- 359 3. Weimann, S.; Kremer, M.; Plotnik, Y.; Lumer, Y.; Nolte, S.; Makris, K.; Segev, M.;  
360 Rechtsman, M.; Szameit, A. *Nature materials* **2017**, 16, 433.
- 361 4. Zhang, Q.; Yin, K.; Dong, H.; Zhou, Y.; Tan, X.; Yu, K.; Hu, X.; Xu, T.; Zhu, C.; Xia, W.  
362 *Nature communications* **2017**, 8, 14889.
- 363 5. Niu, K.; Xu, Y.; Wang, H.; Ye, R.; Xin, H. L.; Lin, F.; Tian, C.; Lum, Y.; Bustillo, K. C.;  
364 Doeff, M. M. *Science advances* **2017**, 3, e1700921.
- 365 6. Zhang, Q.; Shi, Z.; Yin, K.; Dong, H.; Xu, F.; Peng, X.; Yu, K.; Zhang, H.; Chen, C.-C.;  
366 Valov, I. *Nano letters* **2018**, 18, 5070-5077.
- 367 7. Xia, W.; Zhang, Q.; Xu, F.; Sun, L. *ACS applied materials & interfaces* **2016**, 8, 9170-  
368 9177.
- 369 8. Sun, S.; Yuan, D.; Xu, Y.; Wang, A.; Deng, Z. *ACS nano* **2016**, 10, 3648-3657.
- 370 9. Zhu, F.; Men, L.; Guo, Y.; Zhu, Q.; Bhattacharjee, U.; Goodwin, P. M.; Petrich, J. W.;  
371 Smith, E. A.; Vela, J. *ACS nano* **2015**, 9, 2948-2959.
- 372 10. Syrenova, S.; Wadell, C.; Nugroho, F. A.; Gschneidner, T. A.; Fernandez, Y. A. D.; Nalin,  
373 G.; Świtlik, D.; Westerlund, F.; Antosiewicz, T. J.; Zhdanov, V. P. *Nature materials* **2015**, 14,  
374 1236.
- 375 11. Wang, X.; Swihart, M. T. *Chemistry of Materials* **2015**, 27, 1786-1791.
- 376 12. Poul L. Hansen, J. B. W., Stig Helveg, Jens R. Rostrup-Nielsen, Bjerne S. Clausen and

377 Henrik Topsøe. *Science* **2002**, 295, 2053-2055.  
 378 13. Ringe, E.; Van Duyne, R.; Marks, L. *Nano letters* **2011**, 11, 3399-3403.  
 379 14. Wulff, G. *Zeitschrift für Kristallographie-Crystalline Materials* **1901**, 34, 449-530.  
 380 15. Chen, M.; Wu, B.; Yang, J.; Zheng, N. *Advanced materials* **2012**, 24, 862-879.  
 381 16. Laibinis, P. E.; Whitesides, G. M.; Allara, D. L.; Tao, Y. T.; Parikh, A. N.; Nuzzo, R. G.  
 382 *Journal of the American Chemical Society* **1991**, 113, 7152-7167.  
 383 17. Song, H.; Kim, F.; Connor, S.; Somorjai, G. A.; Yang, P. *The Journal of Physical*  
 384 *Chemistry B* **2005**, 109, 188-193.  
 385 18. Xiong, Y.; Cai, H.; Wiley, B. J.; Wang, J.; Kim, M. J.; Xia, Y. *Journal of the American*  
 386 *Chemical Society* **2007**, 129, 3665-3675.  
 387 19. Huang, X.; Zhang, H.; Guo, C.; Zhou, Z.; Zheng, N. *Angewandte Chemie International*  
 388 *Edition* **2009**, 48, 4808-4812.  
 389 20. Liao, H.-G.; Zherebetsky, D.; Xin, H.; Czarnik, C.; Ercius, P.; Elmlund, H.; Pan, M.;  
 390 Wang, L.-W.; Zheng, H. *Science* **2014**, 345, 916-919.  
 391 21. Ye, X.; Jones, M. R.; Frechette, L. B.; Chen, Q.; Powers, A. S.; Ercius, P.; Dunn, G.;  
 392 Rotskoff, G. M.; Nguyen, S. C.; Adiga, V. P. *Science* **2016**, 354, 874-877.  
 393 22. Storm, A.; Chen, J.; Ling, X.; Zandbergen, H.; Dekker, C. *Nature materials* **2003**, 2,  
 394 537.  
 395 23. Zandbergen, H. W.; van Duuren, R. J.; Alkemade, P. F.; Lientschnig, G.; Vasquez, O.;  
 396 Dekker, C.; Tichelaar, F. D. *Nano letters* **2005**, 5, 549-553.  
 397 24. Fischbein, M. D.; Drndić, M. *Nano letters* **2007**, 7, 1329-1337.  
 398 25. Yu, K.; Zhao, W.; Wu, X.; Zhuang, J.; Hu, X.; Zhang, Q.; Sun, J.; Xu, T.; Chai, Y.; Ding, F.  
 399 *Nano Research* **2018**, 1-12.  
 400 26. Lin, J.; Cretu, O.; Zhou, W.; Suenaga, K.; Prasai, D.; Bolotin, K. I.; Cuong, N. T.; Otani,  
 401 M.; Okada, S.; Lupini, A. R. *Nature nanotechnology* **2014**, 9, 436.  
 402 27. Liu, X.; Xu, T.; Wu, X.; Zhang, Z.; Yu, J.; Qiu, H.; Hong, J.-H.; Jin, C.-H.; Li, J.-X.; Wang,  
 403 X.-R. *Nature communications* **2013**, 4, 1776.  
 404 28. Shen, Y.; Xu, T.; Tan, X.; Sun, J.; He, L.; Yin, K.; Zhou, Y.; Banhart, F.; Sun, L. *Nano*  
 405 *letters* **2017**, 17, 5119-5125.  
 406 29. Tudela, D. *Journal of chemical education* **2008**, 85, 863.  
 407 30. Sang, Y.; Kuai, L.; Chen, C.; Fang, Z.; Geng, B. *ACS Appl Mater Interfaces* **2014**, 6,  
 408 5061-8.

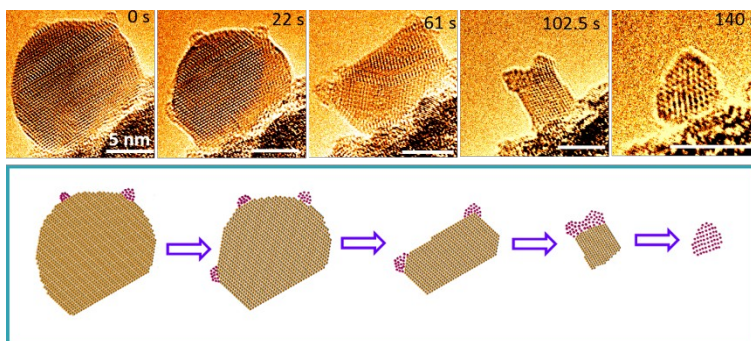
409

410

411

412

TOC



413

